

Tractable Model for Rate in Self-Backhauled Millimeter Wave Cellular Networks

Sarabjot Singh, Mandar N. Kulkarni, Amitava Ghosh, and Jeffrey G. Andrews

Abstract—Millimeter wave (mmW) cellular systems will require high gain directional antennas and dense base station (BS) deployments to overcome high near field path loss and poor diffraction. As a desirable side effect, high gain antennas provide interference isolation, providing an opportunity to incorporate *self-backhauling*—BSs backhauling among themselves in a mesh architecture without significant loss in throughput—to enable the requisite large BS densities. The use of directional antennas and resource sharing between access and backhaul links leads to coverage and rate trends that differ significantly from conventional microwave (μ W) cellular systems. In this paper, we propose a general and tractable mmW cellular model capturing these key trends and characterize the associated rate distribution. The developed model and analysis is validated using actual building locations from dense urban settings and empirically-derived path loss models. The analysis shows that in sharp contrast to the interference limited nature of μ W cellular networks, the *spectral efficiency* of mmW networks (besides total rate) also increases with BS density particularly at the cell edge. Increasing the system bandwidth, although boosting median and peak rates, does not significantly influence the cell edge rate. With self-backhauling, different combinations of the wired backhaul fraction (i.e. the fraction of BSs with a wired connection) and BS density are shown to guarantee the same median rate (QoS).

I. INTRODUCTION

The scarcity of “beachfront” microwave spectrum [1] and surging wireless traffic demands has made going higher in frequency for terrestrial communications inevitable. The capacity boost provided by increased LTE deployments and aggressive small cell, particularly Wi-Fi, offloading has, so far, been able to cater to the increasing traffic demands, but to meet the projected [2] traffic needs of 2020 (and beyond) availability of large amounts of new spectrum would be indispensable. The only place where a significant amount of unused or lightly used spectrum is available is in the millimeter wave (mmW) bands (20 – 100 GHz). With many GHz of spectrum to offer, mmW bands are becoming increasingly attractive as one of the front runners for the next generation (a.k.a. “5G”) wireless cellular networks [3]–[5].

A. Background and recent work

Feasibility of mmW cellular. Although mmW based indoor and personal area networks have already received considerable traction [6], [7], such frequencies have long been deemed unattractive for cellular communications primarily due to the

large near-field loss and poor penetration (blocking) through concrete, water, foliage, and other common material. Recent research efforts [4], [8]–[14] have, however, seriously challenged this widespread perception. In principle, the smaller wavelengths associated with mmW allow placing many more miniaturized antennas in the same physical area, thus compensating for the near-field path loss [8], [9]. Communication ranges of 150-200m have been shown to be feasible in dense urban scenarios with the use of such high gain directional antennas [4], [9], [10]. Although mmW signals do indeed penetrate and diffract poorly through urban clutter, dense urban environments offer rich multipath (at least for outdoor) with strong reflections; making non-line-of-sight (NLOS) communication feasible with familiar path loss exponents in the range of 3-4 [4], [9]. Dense and directional mmW networks have been shown to exhibit a similar spectral efficiency to 4G (LTE) networks (of the same density) [11], [12], and hence can achieve an order of magnitude gain in throughput due to the increased bandwidth.

Coverage trends in mmW cellular. With high gain directional antennas and newfound sensitivity to blocking, mmW coverage trends will be quite different from previous cellular networks. Investigations via detailed system level simulations [11]–[15] have shown large bandwidth mmW networks in urban settings¹ tend to be noise limited—i.e. thermal noise dominates interference—in contrast to 4G cellular networks, which are usually strongly interference limited. As a result, mmW outages are mostly due to a low signal-to-noise-ratio (SNR) instead of low signal-to-interference-ratio (SIR). This insight was also highlighted in an earlier work [16] for directional mmW ad hoc networks. Because cell edge users experience low SNR and are power limited, increased bandwidth leads to little or no gain in their rates as compared to the median or peak rates [12]. Note that rates were compared with a 4G network in [12], however, in this paper we also investigate effect of bandwidth on rate in mmW regime.

Density and backhaul. As highlighted in [8], [11]–[15], dense BS deployments are essential for mmW networks to achieve acceptable coverage and rate. This poses a particular challenge for the backhaul network, especially given the huge rates stemming from mmW bandwidths on the order of GHz. However, the interference isolation provided by narrow directional beams provides a unique opportunity for organic and scalable backhaul architectures [8], [17], [18]. Specifically, *self-backhauling* is a natural and scalable solution [17]–[19],

This work has been supported by Nokia. S. Singh, M. N. Kulkarni, and J. G. Andrews are with Wireless Networking and Communications Group (WNCG), The University of Texas at Austin and A. Ghosh is with Nokia (email: sarabjot@utexas.edu, kulkarni.mandar.n@gmail.com, amitava.ghosh@nsn.com, and jandrews@ece.utexas.edu).

¹Note that capacity crunch is also most severe in such dense urban scenarios.

where BSs with wired backhaul provide for the backhaul of BSs without it using a mmW link. This architecture is quite different from the mmW based point-to-point backhaul [20] or the relaying architecture [21] already in use, as (a) the BS with wired backhaul serves multiple BSs, and (b) access and backhaul link share the total pool of available resources at each BS. This results in a multihop network, but one in which the hops need not interfere, which is what largely doomed previous attempts at mesh networking. However, both the load on the backhaul and access link impact the eventual user rate, and a general and tractable model that integrates the backhauling architecture into the analysis of a mmW cellular network seems important to develop. The main objective of this work is to address this. As we show, the very notion of a coverage/association cell is strongly questionable due to the sensitivity of mmW to blocking in dense urban scenarios. Characterizing the load and rate in such networks, therefore, is non-trivial due to the formation of irregular and “chaotic” association cells (see Fig. 3).

Relevant models. Recent work in developing models for the analysis of mmW cellular networks (ignoring backhaul) includes [22]–[24], where the downlink SINR distribution is characterized assuming BSs to be spatially distributed according to a Poisson point process (PPP). No blockages were assumed in [22], while [23] proposed a line of sight (LOS) ball based blockage model in which all nearby BSs were assumed LOS and all BSs beyond a certain distance from the user were ignored. This blockage model can be interpreted as a step function approximation of the exponential blockage model proposed in [25] and used in [24]. Coverage was shown [23] to improve with antenna directionality, and to exhibit a non-monotonic trend with BS density. In this work, however, we show that if the finite user population is taken into account (ignored in [23]), SINR coverage increases monotonically with density. Although characterizing SINR is important, rate is the key metric, and can follow quite different trends [26], [27] than SINR because the user load is essentially a pre-log factor whereas SINR is inside the log in the Shannon capacity formula.

B. Contributions

The major contributions of this paper can be categorized broadly as follows:

Tractable mmW cellular model. A tractable and general model is proposed in Sec. II for characterizing uplink and downlink coverage and rate distribution in self-backhauled mmW cellular networks. The proposed blockage model allows for an adaptive fraction of area around each user to be LOS. Assuming the BSs are distributed according to a PPP, the analysis, developed in Sec. III, accounts for different path losses (both mean and variance) of LOS/NLOS links for both access and backhaul—consistent with empirical studies [4], [14]. We identify and characterize two types of association cells in self-backhauled networks: (a) *user association area* of a BS which impacts the load on the access link, and (b) *BS association area* of a BS with wired backhaul required for quantifying the load on the backhaul link. The rate distribution

across the entire network, accounting for the random backhaul and access link capacity, is then characterized in Sec. III. Further, the analysis is extended to derive the rate distribution with offloading to and from a co-existing μ W macrocellular network.

Validation of model and analysis. In Sec. III-E, the analytical rate distribution derived from the proposed model is compared with that obtained from simulations employing actual building locations in dense urban regions of New York [28] and Chicago [29], and empirically measured path loss models [14]. The demonstrated close match between the analysis and simulation validates the proposed blockage model and our analytical approximation of the irregular association areas and load.

Performance insights. Using the developed framework, it is demonstrated in Sec. IV that:

- MmW networks in dense urban scenarios employing high gain narrow beam antennas tend to be noise limited for “practical” BS densities. Consequently, densification of the network improves the SINR coverage, especially for uplink. Incorporating the impact of finite user density, SINR coverage is shown to monotonically increase with density even in the very large density regime.
- Cell edge users experience poor SNR and hence are particularly power limited. Increasing the air interface bandwidth, as a result, does not significantly improve the cell edge rate, in contrast to the cell median or peak rates. Improving the density, however, improves the cell edge rate drastically. Assuming all users to be mmW capable, cell edge rates are also shown to improve by reverting users to the μ W network whenever reliable mmW communication is unfeasible.
- Self-backhauling is attractive due to the diminished effect of interference in such networks. Increasing the fraction of BSs with wired backhaul, obviously, improves the peak rates in the network. Increasing the density of BSs while keeping the density of wired backhaul BSs constant in the network, however, leads to saturation of user rate coverage. We characterize the corresponding *saturation density* as the BS density beyond which marginal improvement in rate coverage would be observed without further wired backhaul provisioning. The saturation density is shown to be proportional to the density of BSs with wired backhaul.
- The same rate coverage/median rate is shown to be achievable with various combinations of (i) the fraction of wired backhaul BSs and (ii) the density of BSs. A rate-density-backhaul contour is characterized, which shows, for example, that the same median rate can be achieved through a higher fraction of wired backhaul BSs in sparse networks or a lower fraction of wired backhaul BSs in dense deployments.

II. SYSTEM MODEL

A. Spatial locations

The mmW BSs in the network are assumed to be distributed uniformly in \mathbb{R}^2 as an homogeneous PPP Φ of density (inten-

sity) λ . The PPP assumption is taken for tractability, however other spatial models can be expected to exhibit similar trends due to the nearly constant SINR gap over that of the PPP [30]. The users are also assumed to be uniformly distributed as a PPP Φ_u of density (intensity) λ_u in \mathbb{R}^2 . A fraction ω of the BSs (called anchored BS or A-BS henceforth) have wired backhaul and the rest of BSs backhaul wirelessly to A-BSs. So, the A-BSs serve the rest of the BSs in the network resulting in two-hop links to the users associated with the BSs. Independent *marking* assigns wired backhaul (or not) to each BS and hence the resulting independent point process of A-BSs Φ_w is also a PPP with density $\lambda\omega$. A fraction $\frac{\mu}{\lambda}$ (assigned by independent marking) of the BSs are assumed to form the μ W macrocellular network and thus the corresponding PPP Φ_μ is of density μ .

Notation is summarized in Table I. Capital roman font is used for parameters and italics for random variables.

B. Propagation assumptions

For mmW transmission, the power received at $y \in \mathbb{R}^2$ from a transmitter at $x \in \mathbb{R}^2$ transmitting with power $P(x)$ is given by $P(x)\psi(x, y)L(x, y)^{-1}$, where ψ is the combined antenna gain of the receiver and transmitter and L (dB) = $\beta + 10\alpha \log_{10} \|x - y\| + \chi$ is the associated path loss in dB, where $\chi \sim \mathcal{N}(0, \xi^2)$. Different strategies can be adopted for formulating the path loss model from field measurements. If β is constrained to be the path loss at a close-in reference distance, then α is physically interpreted as the path loss exponent. But if these parameters are obtained by a best linear fit, then β is the intercept and α is the slope of the fit, and no physical interpretation may be ascribed. The deviation in fitting (in dB scale) is modeled as a zero mean Gaussian (Lognormal in linear scale) random variable χ with variance ξ^2 . Motivated by the studies in [4], [14], which point to different LOS and NLOS path loss parameters for access (BS-user) and backhaul (BS-A-BS) links, the analytical model in this paper accommodates distinct β , α , and ξ^2 for each. Each mmW BS and user is assumed to transmit with power P_b and P_u , respectively, over a bandwidth B . The transmit power and bandwidth for μ W BS is denoted by P_μ and B_μ respectively.

All mmW BSs are assumed to be equipped with directional antennas with a sectorized gain pattern. Antenna gain pattern for a BS as a function of angle θ about the steering angle is given by

$$G_b(\theta) = \begin{cases} G_{\max} & \text{if } |\theta| \leq \theta_b \\ G_{\min} & \text{otherwise.} \end{cases},$$

where θ_b is the beam-width or main lobe width. Similar abstractions have been used in the prior study of directional ad hoc networks [31], cellular networks [32], and recently mmW networks [22], [23]. The user antenna gain pattern $G_u(\theta)$ can be modeled in the same manner; however, in this paper we assume omnidirectional antennas for the users. The beams of all non-intended links are assumed to be randomly oriented with respect to each other and hence the effective antenna gains (denoted by ψ) on the interfering links are random. The antennas beams of the intended access and backhaul link are

TABLE I: Notation and simulation parameters

Notation	Parameter	Value (if applicable)
Φ, λ	mmW BS PPP and density	
ω	Anchor BS (A-BS) fraction	
Φ_u, λ_u	user PPP and density	$\lambda_u = 1000$ per sq. km
Φ_μ, μ	μ W BS PPP and density	$\mu = 5$ per sq. km
B	mmW bandwidth	2 GHz
B_μ	μ W bandwidth	20 MHz
P_b	mmW BS transmit power	30 dBm
P_u	user transmit power	20 dBm
ξ	standard deviation of path loss	Access: LOS = 4.9, NLOS = 7.6 Backhaul: LOS = 4.1, NLOS = 7.9
α	path loss exponent	Access: LOS = 2.1, NLOS = 3.3 Backhaul: LOS = 2, NLOS = 3.5 [14]
ν	mmW carrier frequency	73 GHz
β	path loss at 1 m	70 dB
$G_{\max}, G_{\min}, \theta_b$	main lobe gain, side lobe gain, beam-width	$G_{\max} = 18$ dB, $G_{\min} = -2$ dB, $\theta_b = 10^\circ$
C, D	fractional LOS area C in corresponding ball of radius D	0.12, 200 m
σ_N^2	noise power	thermal noise power plus noise figure of 10 dB

assumed to be aligned, i.e., the effective gain on the desired access link is G_{\max} and on the desired backhaul link is G_{\max}^2 . Analyzing the impact of alignment errors on the desired link is beyond the scope of the current work, but can be done on the lines of the recent work [33]. It is worth pointing out here that since our analysis is restricted to 2-D, the directivity of the antennas is modeled only in the azimuthal plane, whereas in practice due to the 3-D antenna gain pattern [9], [14], the RF isolation to the unintended receivers would also be provided by differences in elevation angles.

C. Blockage model

Each access link of separation d is assumed to be LOS with probability C if $d \leq D$ and 0 otherwise². The parameter C should be physically interpreted as the average fraction of LOS area in a circular ball of radius D around the point under consideration. The proposed approach is simple yet flexible enough to capture blockage statistics of real settings as shown in Sec. III-E. The insights presented in this paper corroborate those from other blockage models too [12], [14], [23]. The parameters (C, D) are geography and deployment dependent (low for dense urban, high for semi-urban). The analysis in this paper allows for different (C, D) pairs for access and backhaul links.

D. Association rule

Users are assumed to be associated (or served) by the BS offering the minimum path loss. Therefore, the BS serving the user at origin is $X^*(0) \triangleq \arg \min_{X \in \Phi} L_a(X, 0)$, where 'a' ('b') is for access (backhaul). The index 0 is dropped

²A fix LOS probability beyond distance D can also be handled as shown in Appendix A.

$$\text{Rate} = \begin{cases} \frac{B}{N_{u,w} + \kappa N_b} \log(1 + \text{SINR}_a) & \text{if associated with an A-BS,} \\ \frac{B}{N_u} \min \left(\left(1 - \frac{\kappa}{\kappa N_b + N_{u,w}} \right) \log(1 + \text{SINR}_a), \frac{\kappa}{\kappa N_b + N_{u,w}} \log(1 + \text{SINR}_b) \right) & \text{otherwise.} \end{cases} \quad (1)$$

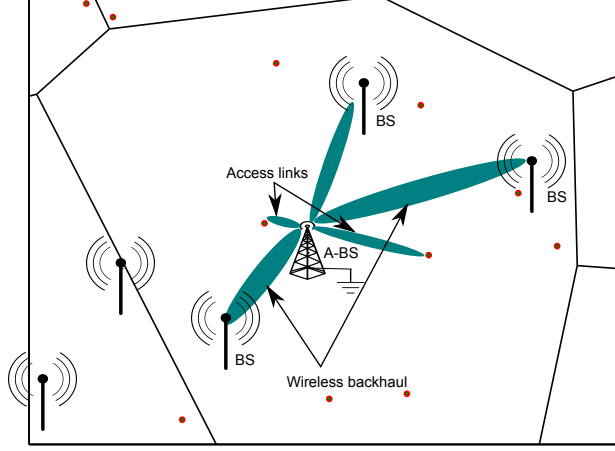


Fig. 1: Self-backhauled network with the A-BS providing the wireless backhaul to the associated BSs and access link to the associated users (denoted by circles). The solid lines depict the regions in which all BSs are served by the A-BS at the center.

henceforth wherever implicit. The analysis in this paper is done for the user located at the origin referred to as the *typical* user³ and its serving BS is the *tagged* BS. Further, each BS (with no wired backhaul) is assumed to be backhauled over the air to the A-BS offering the lowest path loss to it. Thus, the A-BS (tagged A-BS) serving the tagged BS at X^* (if not an A-BS itself) is $Y^*(X^*) \triangleq \arg \min_{Y \in \Phi_w} L_b(Y, X^*)$, with $X^* \notin \Phi_w$. This two-hop setup is demonstrated in Fig. 1. As a result, the access (downlink and uplink), and backhaul link SINR are

$$\text{SINR}_d = \frac{P_b G_{\max} L_a(X^*)^{-1}}{I_d + \sigma_N^2}, \quad \text{SINR}_u = \frac{P_u G_{\max} L_a(X^*)^{-1}}{I_u + \sigma_N^2},$$

$$\text{SINR}_b = \frac{P_b G_{\max}^2 L_b(X^*, Y^*)^{-1}}{I_b + \sigma_N^2},$$

respectively, where $\sigma_N^2 \triangleq N_0 B$ is the thermal noise power and $I_{(\cdot)}$ is the corresponding interference.

E. Validation methodology

The analytical model and results presented in this paper are validated using Monte Carlo simulations employing actual building topology of two major metropolitan areas, Manhattan and Chicago, obtained from [28] and [29] respectively. The polygons representing the buildings in the corresponding regions are shown in Fig. 2. These regions represent dense urban settings, where mmW networks are most attractive. In each simulation trial, users and BSs are dropped randomly in these geographical areas as per the corresponding densities.

³Notion of typicality is enabled by Slivnyak's theorem [34].

Users are dropped only in the outdoor regions, whereas the BSs landing inside a building polygon are assumed to be NLOS to all users. A BS-user link is assumed to be NLOS if a building blocks the line segment joining the two, and LOS otherwise. The association and propagation rules are assumed as described in the earlier sections. The specific path loss parameters used are listed in Table I and are from empirical measurements [14]. The association cells formed by two different placements of mmW BSs in downtown Manhattan with this methodology are shown in Fig. 3.

F. Access and backhaul load

Access and backhaul links are assumed to share the same pool of radio resources and hence the user rate depends on the user load at BSs and BS load at A-BSs. Let N_b , $N_{u,w}$, and N_u denote the number of BSs associated with the tagged A-BS, number of users served by the tagged A-BS, and the number of users associated with the tagged BS respectively. By definition, when the typical user associates with an A-BS, $N_{u,w} = N_u$. Since an A-BS serves both users and BSs, the resources allocated to the associated BSs (which further serve their associated users) are assumed to be proportional to their average user load. Let the average number of users per BS be denoted by $\kappa \triangleq \lambda_u / \lambda$, and then the fraction of resources η_b available for all the associated BSs at an A-BS are $\frac{\kappa N_b}{\kappa N_b + N_{u,w}}$, and those for the access link with the associated users are then $\eta_{a,w} = 1 - \eta_b = \frac{N_{u,w}}{\kappa N_b + N_{u,w}}$. The fraction of resources reserved for the associated BSs at an A-BS are assumed to be shared equally among the BSs and hence the fraction of resources available to the tagged BS from the tagged A-BS are η_b / N_b , which is equivalent to the resource fraction used for backhaul by the corresponding BS. The access and backhaul capacity at each BS is assumed to be shared equally among the associated users.

With the above described resource allocation model the rate/throughput of a user is given by (1) (at top of this page), where SINR_a corresponds to the SINR of the access link: $a \equiv d$ for downlink and $a \equiv u$ for uplink.

G. Hybrid networks

Co-existence with conventional μW based 3G and 4G networks could play a key role in providing wide coverage, particularly in sparse deployment of mmW networks, and reliable control channels. In this paper, a *simple* offloading technique is adopted wherein a user is offloaded to the μW network if its SINR on the mmW network drops below a threshold τ_{\min} . Although an SINR based offloading strategy is highly suboptimal for μW HetNets [27], due to the large bandwidth disparity between the mmW and μW network it is arguably reasonable in mmW [26], [35].

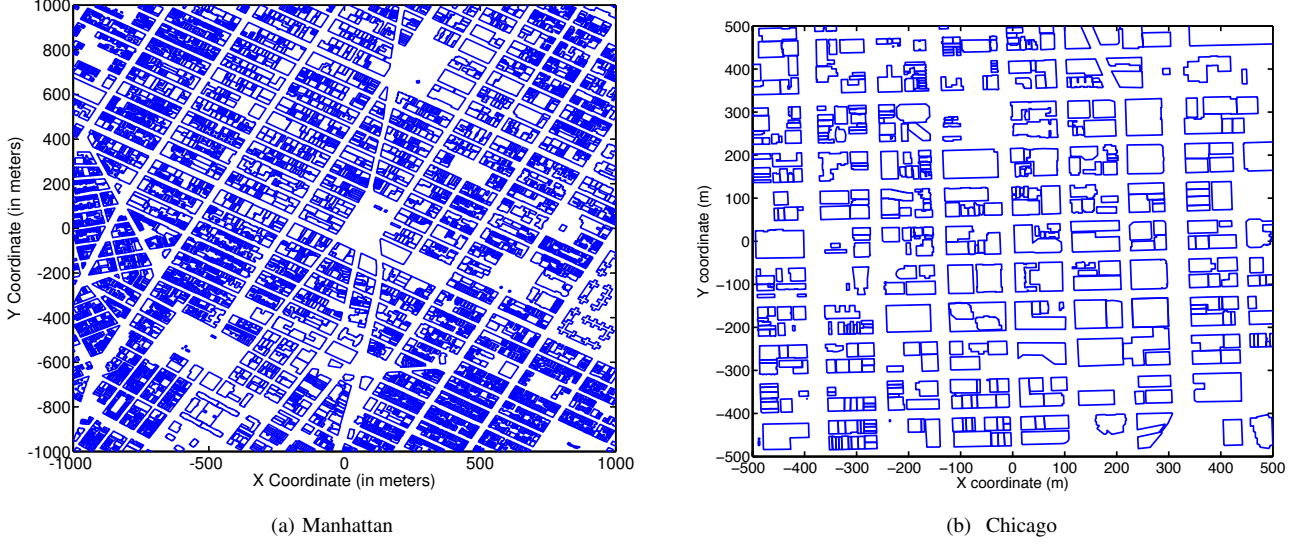


Fig. 2: Building topology of Manhattan and Chicago used for validation.

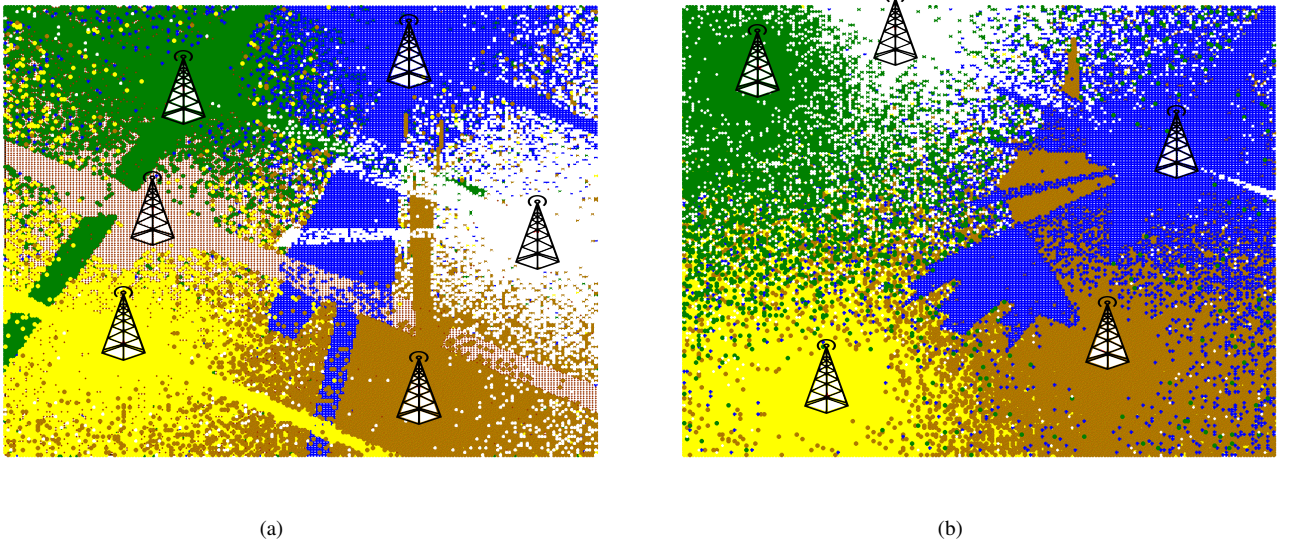


Fig. 3: Association cells in different shades and colors in Manhattan for two different BS placement. Noticeable discontinuity and irregularity of the cells show the sensitivity of path loss to blockages and the dense building topology (shown in Fig. 2a).

III. RATE DISTRIBUTION: DOWNLINK AND UPLINK

This is the main technical section of the paper, which characterizes the user rate distribution across the network in a self-backhauled mmW network co-existing with a μ W macrocellular network.

A. SNR distribution

For characterizing the downlink SNR distribution, the point process formed by the path loss of each BS to the typical user at origin defined as $\mathcal{N}_a := \left\{ L_a(X) = \frac{\|X\|^\alpha}{S} \right\}_{X \in \Phi}$, where $S \triangleq 10^{-(\chi+\beta)/10}$, on \mathbb{R} is considered. Using the displacement theorem [34], \mathcal{N}_a is a Poisson process and let the corresponding intensity measure be denoted by $\Lambda_a(\cdot)$.

Lemma 1. *The distribution of the path loss from the user to the tagged base station is such that $\mathbb{P}(L_a(X^*) > t) = \exp(-\Lambda_a((0, t]))$, where the intensity measure is given by*

$$\begin{aligned} \Lambda_a((0, t]) = & \lambda \pi C \left\{ D^2 \left[Q \left(\frac{\ln(D^{\alpha_l}/t) - m_l}{\sigma_l} \right) - Q \left(\frac{\ln(D^{\alpha_n}/t) - m_n}{\sigma_n} \right) \right] \right. \\ & + t^{2/\alpha_l} \exp \left(2 \frac{\sigma_l^2}{\alpha_l^2} + 2 \frac{m_l}{\alpha_l} \right) Q \left(\frac{\sigma_l^2(2/\alpha_l) - \ln(D^{\alpha_l}/t) + m_l}{\sigma_l} \right) \\ & \left. + t^{2/\alpha_n} \exp \left(2 \frac{\sigma_n^2}{\alpha_n^2} + 2 \frac{m_n}{\alpha_n} \right) \left[\frac{1}{C} - Q \left(\frac{\sigma_n^2(2/\alpha_n) - \ln(D^{\alpha_n}/t) + m_n}{\sigma_n} \right) \right] \right\}, \end{aligned} \quad (2)$$

where $m_j = -0.1\beta_j \ln 10$, $\sigma_j = 0.1\xi_j \ln 10$, with $j \equiv l$ for LOS and $j \equiv n$ for NLOS, and $Q(\cdot)$ is the Q-function (Normal Gaussian CCDF).

Proof: See Appendix A. ■

The path loss distribution for a typical backhaul link can

$$M'(t) \triangleq \frac{dM(t)}{dt} = \pi C \left\{ \frac{D^2}{\sqrt{2\pi\sigma_l^2 t}} \left[\exp\left(-\left(\frac{\ln(D^{\alpha_l}/t) - m_l}{\sqrt{2\sigma_l^2}}\right)^2\right) - \exp\left(-\left(\frac{\ln(D^{\alpha_n}/t) - m_n}{\sqrt{2\sigma_n^2}}\right)^2\right) \right] + \right. \\ \left. \exp\left(2\frac{\sigma_l^2}{\alpha_l^2} + 2\frac{m_l}{\alpha_l}\right) t^{\frac{2}{\alpha_l}-1} \left[\frac{2}{\alpha_l} Q\left(\frac{\sigma_l^2(2/\alpha_l) - \ln(D^{\alpha_l}/t) + m_l}{\sigma_l}\right) - \frac{1}{\sqrt{2\pi\sigma_l^2}} \exp\left(-\left(\frac{\sigma_l^2(2/\alpha_l) - \ln(D^{\alpha_l}/t) + m_l}{\sqrt{2\sigma_l^2}}\right)^2\right) \right] + \right. \\ \left. \exp\left(2\frac{\sigma_n^2}{\alpha_n^2} + 2\frac{m_n}{\alpha_n}\right) t^{\frac{2}{\alpha_n}-1} \left[\frac{2}{\alpha_n} Q\left(\frac{\sigma_n^2(2/\alpha_n) - \ln(D^{\alpha_n}/t) + m_n}{\sigma_n}\right) + \frac{1}{\sqrt{2\pi\sigma_n^2}} \exp\left(-\left(\frac{\sigma_n^2(2/\alpha_n) - \ln(D^{\alpha_n}/t) + m_n}{\sqrt{2\sigma_n^2}}\right)^2\right) \right] \right\}. \quad (4)$$

be similarly obtained by considering the propagation process [36] \mathcal{N}_b from A-BSs to the BS at the origin. The corresponding intensity measure Λ_b is then obtained by replacing λ by $\lambda\omega$ and replacing the access link parameters with that of backhaul link in (2).

Under the assumptions of stationary PPP for both users and BSs, considering the typical link for analysis allows characterization of the corresponding network-wide performance metric. Therefore, the SNR coverage defined as the distribution of SNR for the typical link $\mathcal{S}_{(\cdot)}(\tau) \triangleq \mathbb{P}_{\Phi_u}^o(\text{SNR}_{(\cdot)} > \tau)$ ⁴ is also the complementary cumulative distribution function (CCDF) of SNR across the entire network. The same holds for SINR and Rate coverage.

Lemma 1 enables the characterization of SNR distribution in a closed form in the following theorem.

Theorem 1. *The SNR distribution for the typical downlink, uplink, and backhaul link are respectively*

$$\begin{aligned} \mathcal{S}_d(\tau) &\triangleq \mathbb{P}(\text{SNR}_d > \tau) = 1 - \exp\left(-\lambda M_a\left(\frac{P_b G_{\max}}{\tau \sigma_N^2}\right)\right) \\ \mathcal{S}_u(\tau) &\triangleq \mathbb{P}(\text{SNR}_u > \tau) = 1 - \exp\left(-\lambda M_a\left(\frac{P_u G_{\max}}{\tau \sigma_N^2}\right)\right) \\ \mathcal{S}_b(\tau) &\triangleq \mathbb{P}(\text{SNR}_b > \tau) = 1 - \exp\left(-\lambda \omega M_b\left(\frac{P_b G_{\max}^2}{\tau \sigma_N^2}\right)\right), \end{aligned}$$

where $M_a(t) \triangleq \frac{\Lambda_a((0,t])}{\lambda}$ and $M_b(t) \triangleq \frac{\Lambda_b((0,t])}{\lambda\omega}$.

Proof: For the downlink case,

$$\begin{aligned} \mathbb{P}(\text{SNR}_d > \tau) &= \mathbb{P}\left(\frac{P_b G_{\max} L_a(X^*)^{-1}}{\sigma_N^2} > \tau\right) \\ &= 1 - \exp\left(-\lambda M_a\left(\frac{P_b G_{\max}}{\tau \sigma_N^2}\right)\right), \end{aligned}$$

where the last equality follows from Lemma 1. Uplink and backhaul link coverage follow similarly. ■

B. Interference in mmW networks

This section provides an analytical treatment of interference in mmW networks. In particular, the focus of this section is to upper bound the interference-to-noise (INR) distribution (both uplink and downlink) and hence provide more insight into an earlier comment of noise limited nature ($\text{SNR} \approx \text{SINR}$) of

mmW networks. Without any loss of generality, each BS is assumed to be an A-BS (i.e. $\omega = 1$) in this section and hence the subscript ‘a’ for access is dropped.

Consider the sum over the earlier defined PPP \mathcal{N}

$$I_t \triangleq \sum_{Y \in \mathcal{N}} Y^{-1} K_Y, \quad (3)$$

where K_Y are i.i.d. marks associated with $Y \in \mathcal{N}$. For example, if $K_Y = P_b \psi_Y$ with ψ_Y being the random antenna gain on the link from Y , then I_t denotes the total received power from all BSs. The following proposition provides an upper bound to interference in mmW networks.

Proposition 1. *The CCDF of INR is upper bounded as*

$$\mathbb{P}(\text{INR} > y) \leq \frac{2e^{a\sigma_N^2 y}}{\pi} \int_0^\infty \text{Re}(\bar{\mathcal{L}}_{I_t}(a + iu)) \cos u \sigma_N^2 y du,$$

where $\bar{\mathcal{L}}_{I_t}(z) = 1/z - \mathcal{L}_{I_t}(z)/z$ with

$$\mathcal{L}_{I_t}(z) = \exp\left(-\lambda \mathbb{E}_K \left[z K \int_{u>0} (1 - \exp(-u)) M'(zK/u)/u^2 du \right]\right)$$

and M' is given by (4) (at top of page).

Proof: The downlink interference $I_d = I_t - K_{X^*}/X^*$ is clearly upper bounded by I_t and hence $\text{INR} \triangleq I_d/\sigma_N^2$ has the property: $\mathbb{P}(\text{INR} > y) \leq \mathbb{P}(I_t > \sigma_N^2 y)$. The sum in (3) is the shot noise associated with \mathcal{N} and the corresponding Laplace transform is represented as the Laplace functional of the shot noise of \mathcal{N} , $\mathcal{L}_{I_t}(z) \triangleq \mathbb{E}[\exp(-zI_t)]$

$$= \exp\left(-\mathbb{E}_K \left[\int_{y>0} \{1 - \exp(-zK/y)\} \Lambda(dy) \right]\right),$$

and the Laplace transform associated with the CCDF of the shot noise is $\bar{\mathcal{L}}_{I_t}(z) = 1/z - \mathcal{L}_{I_t}(z)/z$. The CCDF of the shot noise can then be obtained from the corresponding Laplace transform using the Euler characterization [37]

$$\bar{F}_{I_t}(y) \triangleq \mathbb{P}(I_t > y) = \frac{2e^{ay}}{\pi} \int_0^\infty \text{Re}(\bar{\mathcal{L}}_{I_t}(a + iu)) \cos uy du. \quad \blacksquare$$

Remark 1. Density-Directivity Equivalence. *For the special case of uniform path loss exponent and shadowing variance for all links, $M(u) = \pi \mathbb{E}[S^{2/\alpha}] u^{2/\alpha}$ and $M'(u) =$*

⁴ \mathbb{P}_{Φ}^o is the Palm probability associated with the corresponding PPP Φ . This notation is omitted henceforth with the implicit understanding that when considering the typical link, Palm probability is being referred to.

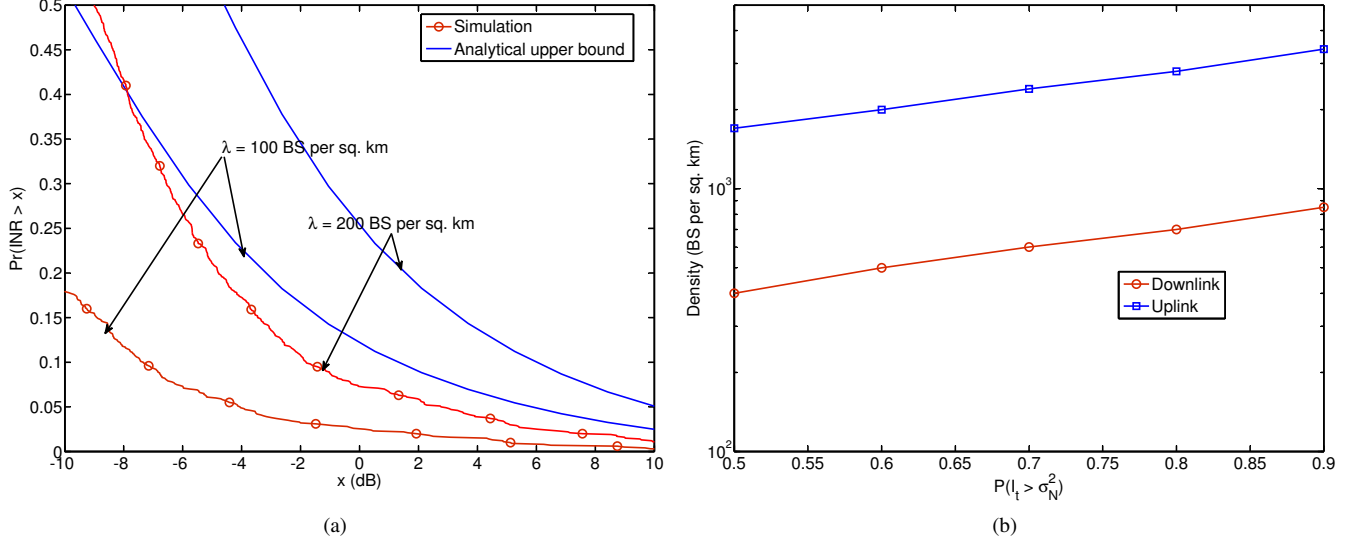


Fig. 4: (a) Total power to noise ratio and INR for the proposed model, and (b) the variation of the density required for the total power to exceed noise with a given probability.

$\frac{2\pi}{\alpha} \mathbb{E} [S^{2/\alpha}] u^{2/\alpha-1}$, the Laplace transform of I_t is

$$\begin{aligned} & \exp \left(-2\pi \frac{\lambda}{\alpha} \mathbb{E} [S^{2/\alpha}] \mathbb{E}_K \left[\int_{u>0} (1 - \exp(-zK/u)) u^{2/\alpha-1} du \right] \right) \\ &= \exp \left(2\pi \frac{\lambda}{\alpha} z^{2/\alpha} \mathbb{E} [S^{2/\alpha}] \mathbb{E} [K^{2/\alpha}] \Gamma \left(\frac{-2}{\alpha} \right) \right) \\ &= \exp \left(2\pi \frac{\lambda}{\alpha} z^{2/\alpha} \mathbb{E} [(SP)^{2/\alpha}] \mathbb{E} [\psi^{2/\alpha}] \Gamma \left(\frac{-2}{\alpha} \right) \right). \end{aligned}$$

As can be noted from above, the interference distribution depends on the product of $\lambda \mathbb{E} [\psi^{2/\alpha}]$, which implies networks with higher directivity (low $\mathbb{E} [\psi^{2/\alpha}]$) and high density have the same total power distribution as that of a network with less directivity and low density.

The interference on the uplink is generated by users transmitting on the same radio resource as the typical user. Assuming each BS gives orthogonal resources to users associated with it, one user per BS would interfere with the uplink transmission of the typical user. The point process of the interfering users, for the analysis in this section, is assumed to be a PPP $\Phi_{u,b}$ of intensity same as that of BSs, i.e., λ . In the same vein as in the above discussion, the propagation process $\mathcal{N}_u := \{L_a(X)\}_{X \in \Phi_{u,b}}$ captures the propagation loss from users to the BS under consideration at origin. The shot noise $I_t \triangleq \sum_{U \in \mathcal{N}_u} U^{-1} K_U$ then upper bounds the uplink interference with $K_U = P_u \psi_U$.

The analytical total power to noise ratio bound for the downlink with the parameters of Table I is shown in Fig. 4a. The Matlab code for computing the upper bound is available online [38]. Also shown is the corresponding INR obtained through simulations. As can be observed from the analytical upper bounds and simulation, the interference does not dominate noise power. In fact, $\text{INR} > 0$ dB is observed in less than 20% of the cases even at high base station densities of about 200 per sq. km. Due to the mentioned stochastic dominance, the distribution of the total power (derived above) can be used to

lower bound the density required for interference to dominate noise. The minimum density required for achieving a given $\Pr(I_t > \sigma_N^2)$ for uplink and downlink is shown in Fig. 4b. As can be seen, a density of at least 500 and 2000 BS per sq. km is required for guaranteeing downlink and uplink interference to exceed noise power with 0.7 probability, respectively.

The SINR distribution of the typical link defined as $\mathcal{P}_{(\cdot)}(\tau) \triangleq \mathbb{P}^o_{\Phi_u}(\text{SINR}_{(\cdot)} > \tau)$ can be derived using the intensity measure of Lemma 1 and is delegated to Appendix B. However, as shown in this section, SNR provides a good approximation to SINR for directional mmW networks in densely blocked settings (typical for urban settings), and hence the following analysis would, *deliberately*, ignore interference (i.e. $\mathcal{P} = \mathcal{S}$), however the corresponding simulation results include interference, thereby validating this assumption.

C. Load characterization

As mentioned earlier, throughput on access and backhaul link depends on the number of users sharing the access link and the number of BSs backhauling to the same A-BS respectively. Hence there are two types of association cells in the network: 1) user association cell of a BS—the region in which all users are served by the corresponding BS, and 2) BS association cell of an A-BS—the region in which all BSs are served by that A-BS. Formally, the user association cell of a BS (or an A-BS) located at $X \in \mathbb{R}^2$ is

$$\mathcal{C}_X = \{Y \in \mathbb{R}^2 : L_a(X, Y) < L_a(T, Y) \forall T \in \Phi\}$$

and the BS association cell of an A-BS located at $Z \in \mathbb{R}^2$

$$\mathcal{C}_Z = \{Y \in \mathbb{R}^2 : L_b(Z, Y) < L_b(T, Y) \forall T \in \Phi_w\}.$$

Due to the complex associations cells in such networks, the resulting distribution of the association area (required for characterizing load distribution) is highly non-trivial to

$$\begin{aligned} \mathcal{R}(\rho) \triangleq \mathbb{P}(\text{Rate} > \rho) &= \omega \sum_{n \geq 0, m \geq 1} K(\lambda(1-\omega), \lambda\omega, n) K_t(\lambda_u, \lambda, m) \mathcal{S}_d(v\{\hat{\rho}(\kappa n + m)\}) \\ &+ (1-\omega) \sum_{l \geq 1, n \geq 1, m \geq 0} K_t(\lambda_u, \lambda, l) K_t(\lambda(1-\omega), \omega\lambda, n) K(\lambda_u, \lambda, m) \mathcal{S}_b(v\{\hat{\rho}l(n + m/\kappa)\}) \mathcal{S}_d\left(v\left\{\hat{\rho}l \frac{n + m/\kappa}{n + m/\kappa - 1}\right\}\right) \end{aligned} \quad (5)$$

characterize exactly. The corresponding means, however, are characterized exactly by the following remark.

Remark 2. Mean Association Areas. Under the modeling assumptions of Sec. II, the association rule assumed corresponds to a stationary (translation invariant) association [39], and consequently the mean user association area of a typical BS equals the inverse of the corresponding density, i.e., $\frac{1}{\lambda}$, and the mean BS association area of a typical A-BS equals $\frac{1}{\lambda\omega}$.

For the area distribution of association cells and the resulting load, the analytical approximation proposed in [26] is used, where the area of a typical association cell is ascribed a gamma distribution proposed in [40] for a Poisson Voronoi with the same mean area. Note that the user association area of the tagged BS and the BS association area of the tagged A-BS follow an area biased distribution as compared to that of the corresponding typical areas [39]. This is due to the conditioning on the presence of typical user and the tagged BS in the user association cell of the tagged BS and BS association cell of the tagged A-BS respectively. The probability mass function (PMF) of the resulting loads are stated below. The proofs follow similar lines for [26], [41] and are skipped.

Proposition 2. 1) The PMF of the number of users N_u associated with the tagged BS is

$$K_t(\lambda_u, \lambda, n) = \mathbb{P}(N_u = n), \quad n \geq 1,$$

where $K_t(c, d, n)$

$$= \frac{3.5^{3.5}}{(n-1)!} \frac{\Gamma(n+3.5)}{\Gamma(3.5)} \left(\frac{c}{d}\right)^{n-1} \left(3.5 + \frac{c}{d}\right)^{-(n+3.5)},$$

and $\Gamma(x) = \int_0^\infty \exp(-t)t^{x-1}dt$ is the gamma function. The corresponding mean is $\bar{N}_u \triangleq \mathbb{E}[N_u] = 1 + 1.28 \frac{\lambda_u}{\lambda}$ [26]. When the user associates with an A-BS $N_{u,w} = N_u$. Otherwise, the number of users $N_{u,w}$ served by the tagged A-BS follow the same distribution as those in a typical BS given by

$$K(\lambda_u, \lambda, n) = \mathbb{P}(N_{u,w} = n), \quad n \geq 0,$$

where

$$K(c, d, n) = \frac{3.5^{3.5}}{n!} \frac{\Gamma(n+3.5)}{\Gamma(3.5)} \left(\frac{c}{d}\right)^n \left(3.5 + \frac{c}{d}\right)^{-(n+3.5)}.$$

The corresponding mean is $\bar{N}_{u,w} \triangleq \mathbb{E}[N_{u,w}] = \frac{\lambda_u}{\lambda}$.

2) The number of BSs N_b served by the tagged A-BS, when the typical user is served by the A-BS, has the same distribution as the number of BSs associated with a typical A-BS and hence

$$K(\lambda(1-\omega), \lambda\omega, n) = \mathbb{P}(N_b = n), \quad n \geq 0.$$

The corresponding mean is $\bar{N}_b \triangleq \mathbb{E}[N_b] = \frac{1-\omega}{\omega}$. In the scenario where the typical user associates with a BS, the number of BSs N_b associated with the tagged A-BS is given by

$$K_t(\lambda(1-\omega), \omega\lambda, n) = \mathbb{P}(N_b = n), \quad n \geq 1.$$

The corresponding mean is $\bar{N}_b = 1 + 1.28 \frac{1-\omega}{\omega}$.

D. Rate coverage

As emphasized in the introduction, the rate distribution (capturing the impact of loads on access and backhaul links) is vital for assessing the performance of self-backhauled mmW networks. The Lemmas below characterize the downlink rate distribution for a mmW and a hybrid network employing the following approximations. Corresponding results for the uplink are obtained by replacing \mathcal{S}_d with \mathcal{S}_u .

Assumption 1. The number of users N_u served by the tagged BS and the number of BSs N_b served by the tagged A-BS are assumed independent of each other and the corresponding link SINRs/SNRs.

Assumption 2. The spectral efficiency of the tagged backhaul link is assumed to follow the same distribution as that of the typical backhaul link.

Lemma 2. The rate coverage of a typical user in a self backhauled mmW network, described in Sec. II, for a rate threshold ρ is given by (5) (at top of page), where $\hat{\rho} = \rho/B$, $v(x) = 2^x - 1$, and $\mathcal{S}_{(\cdot)}$ are from Theorem 1.

Proof: Let \mathcal{A}_w denote the event of the typical user associating with an A-BS, i.e., $\mathbb{P}(\mathcal{A}_w) = \omega$. Then, using (1), the rate coverage is

$$\begin{aligned} \mathcal{R}(\rho) &= \omega \mathbb{P}\left(\frac{\eta_{a,w}}{N_{u,w}} \log(1 + \text{SINR}_d) > \hat{\rho} | \mathcal{A}_w\right) + (1-\omega) \times \\ &\mathbb{P}\left(\frac{1}{N_u} \min\left(\left(1 - \frac{\eta_b}{N_b}\right) \log(1 + \text{SINR}_d), \frac{\eta_b}{N_b} \log(1 + \text{SINR}_b)\right) > \hat{\rho} | \bar{\mathcal{A}}_w\right) \\ &= \omega \mathbb{E}[\mathcal{S}_d(v\{\hat{\rho}\{N_{u,w} + \kappa N_b\}\})] + (1-\omega) \times \\ &\mathbb{E}\left[\mathcal{S}_d\left(v\left\{\hat{\rho} N_u \frac{N_b + N_{u,w}/\kappa}{N_b + N_{u,w}/\kappa - 1}\right\}\right) \mathcal{S}_b(v\{\hat{\rho} N_u (N_b + N_{u,w}/\kappa)\})\right]. \end{aligned}$$

The rate coverage expression then follows by invoking the independence among various loads and SNRs. ■

In case the different loads in the above Lemma are approximated with their respective means, the rate coverage expression is simplified as in the following Corollary.

Corollary 1. The rate coverage with mean load approximation using Proposition 2 is given by (6) (at top of page).

Remark 3. In practical communications systems, it might be unfeasible to transmit reliably with any modulation and coding

$$\begin{aligned} \bar{\mathcal{R}}(\rho) = & \omega \mathcal{S}_d \left(v \left\{ \hat{\rho} \left(\frac{\lambda_u(1-\omega)}{\lambda\omega} + 1 + 1.28 \frac{\lambda_u}{\lambda} \right) \right\} \right) \\ & + (1-\omega) \mathcal{S}_b \left(v \left\{ \hat{\rho} \left(1 + 1.28 \frac{\lambda_u}{\lambda} \right) \left(2 + 1.28 \frac{1-\omega}{\omega} \right) \right\} \right) \mathcal{S}_d \left(v \left\{ \hat{\rho} \left(1 + 1.28 \frac{\lambda_u}{\lambda} \right) \frac{2 + 1.28(1-\omega)/\omega}{1 + 1.28(1-\omega)/\omega} \right\} \right) \end{aligned} \quad (6)$$

(MCS) below a certain SNR: τ_0 (say), and in that case $\text{Rate} = 0$ for $\text{SNR} < \tau_0$. Such a constraint can be incorporated in the above analysis by replacing $v \rightarrow \max(v, \tau_0)$.

The following Lemma characterizes the rate distribution in a hybrid network with the association technique of Sec. II-G.

Lemma 3. *The rate distribution in a hybrid mmW network co-existing with a μ W macrocellular network, described in Sec. II-G, is*

$$\begin{aligned} \mathcal{R}_H(\rho) = & \mathcal{R}_1(\rho) + (1 - \mathcal{S}_d(\tau_{\min})) \\ & \times \sum_{n \geq 1} \mathbf{K}_t(\lambda_u - \lambda_{u,m}, \mu, n) \mathcal{P}_\mu(v \{ \rho n / B_\mu \}), \end{aligned}$$

where $\mathcal{R}_1(\rho)$ is obtained from Lemma 2 by replacing $\lambda_u \rightarrow \lambda_{u,m} \triangleq \lambda_u \mathcal{S}_d(\tau_{\min})$ (the effective density of users associated with mmW network) and $v \rightarrow v_1 \triangleq \max(v, \tau_{\min})$, \mathcal{P}_μ is the SINR coverage on μ W network, and $\mathbf{K}_t(\lambda_u - \lambda_{u,m}, \mu, n)$ is the PMF of the number of users N_μ associated with the tagged μ W BS.

Proof: Under the association method of Sec. II-G, the rate coverage in the hybrid setting is

$$\begin{aligned} \mathbb{P}(\text{Rate} > \rho) = & \mathbb{P}(\text{Rate} > \rho \cap \text{SINR}_d > \tau_{\min}) \\ & + \mathbb{P}(\text{Rate} > \rho \cap \text{SINR}_d < \tau_{\min}) \\ = & \mathcal{R}_1(\rho) + (1 - \mathcal{S}_d(\tau_{\min})) \mathbb{E}[\mathcal{P}_\mu(v \{ \rho / B_\mu N_\mu \})], \end{aligned}$$

where the first term on the RHS is the rate coverage when associated with the mmW network and hence \mathcal{R}_1 follows from the previous Lemma 2 by incorporating the offloading SNR threshold and reducing the user density to account for the users offloaded to the macrocellular network (fraction $1 - \mathcal{S}_d(\tau_{\min})$). The second term is the rate coverage when associated with the μ W network and N_μ is the load on the tagged μ W BS, whose distribution can be expressed as in [26] noting the mean association cell area of a μ W BS is $\frac{1 - \mathcal{S}_d(\tau_{\min})}{\mu}$. The μ W network's SINR coverage \mathcal{P}_μ can be derived as in earlier work [36], [42]. ■

E. Validation

In the proposed model, the primary geography dependent parameters are C and D. As mentioned earlier, for a given D, the parameter C is the LOS fractional area within distance D. In order to fit the proposed model to a particular geographical region, the following methodology is adopted. Using Monte Carlo simulations in the setup of Sec. II-E, the average fraction of LOS area in a ball of radius D around randomly dropped users is obtained as a function of the radius D. Fig. 5 shows the empirical C obtained by averaging over the Manhattan and Chicago regions of Fig. 2. It can be seen that at an average of

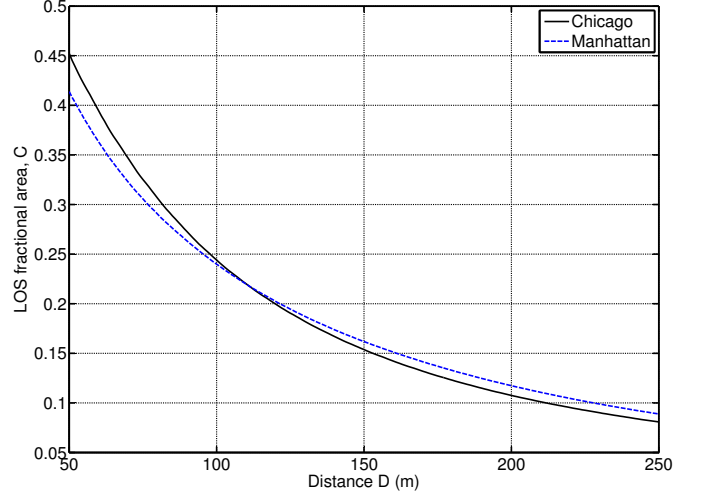


Fig. 5: LOS fractional area as a function of radius D averaged over the respective geographical regions.

TABLE II: Values of D and C

Urban area	D (m)	C
Chicago	250	0.081
Manhattan	200	0.117

about 15% area is LOS in a ball of radius 150m around a user in these regions. The downlink rate distribution (both uplink and downlink) obtained from simulations (as per Sec. II-E) and analysis (Lemma 2) is shown in Fig. 6 for the two cities with two different BS densities. The parameters (C, D) used in analysis for the specific geography are obtained using Fig. 5 and are given in Table II. The closeness of the analytical results to those of the simulations validates (a) the ability of the proposed simple blockage model to capture the blockage characteristics of dense urban settings, and (b) the load characterization for irregular association cells (Fig. 3) in a mmW network. The closeness of the match builds confidence in the model and the derived design insights.

In the above plots any (C, D) pair from Fig. 5 can be used. However, it is observed that the match is better for the (C, D) pair with larger D (200-250m). This is due to the fact that the LOS fractional area (C_2 , say) beyond distance D is ignored, which is a better approximation for larger D. It is straightforward to allow LOS area outside D in the analysis (as shown in Appendix A) but estimating the same using actual building locations is quite computationally intensive and tricky, as averaging needs to be done over a considerably larger area. The fit procedure is simplified, though not sacrificing the accuracy of the fit much (as seen), by setting $C_2 = 0$ in the model.

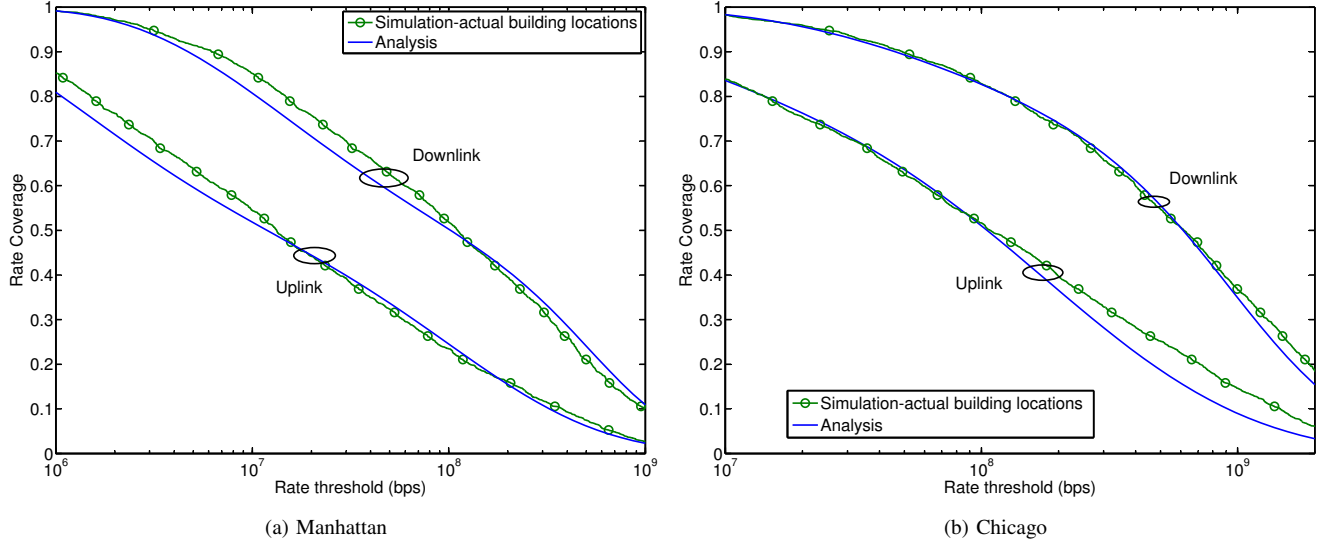


Fig. 6: Downlink rate distribution comparison from simulation and analysis for BS density 30 per sq. km in Manhattan (a) and 60 per sq. km in Chicago (b).

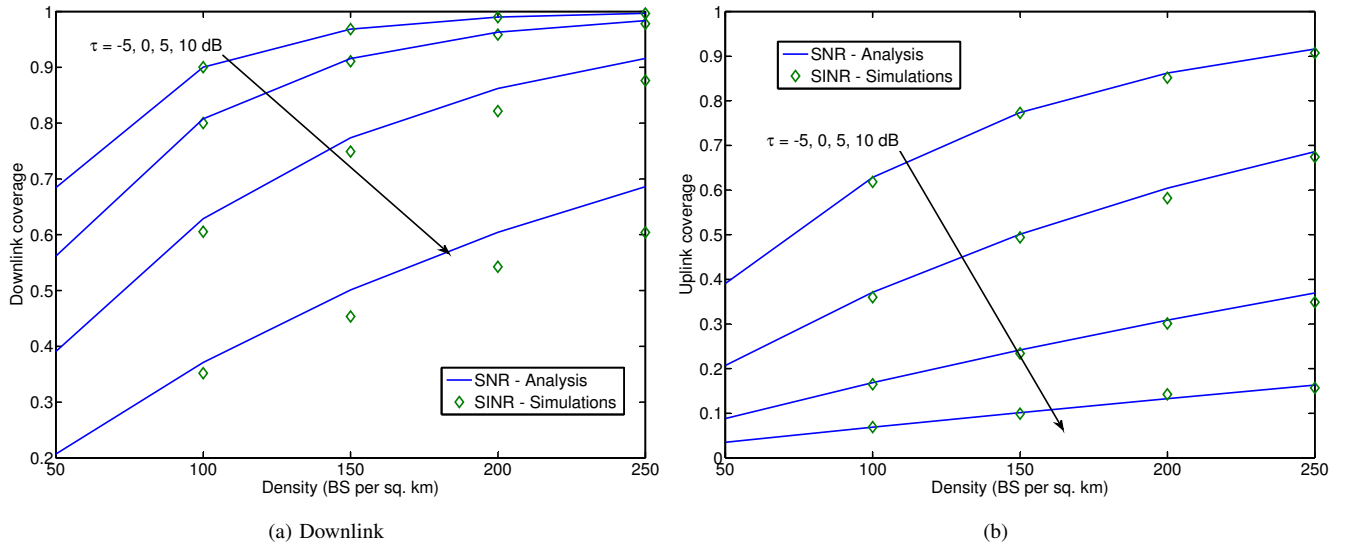


Fig. 7: Comparison of SINR (analysis) and SINR (simulation) coverage with varying BS density.

IV. PERFORMANCE ANALYSIS AND TRENDS

A. Coverage and density

The downlink and uplink coverage for various thresholds and density of BSs is shown in Fig. 7. There are two major observations:

- The analytical SNR tracks the SINR obtained from simulation quite well for both downlink and uplink. A small gap ($< 10\%$) is observed for an example downlink case with larger BS density (250 per sq. km) and a higher threshold of 10 dB.
- Increasing the BS density improves both the downlink and uplink coverage and hence the spectral efficiency—a trend in contrast to conventional interference-limited networks, which are nearly invariant in SINR to density.

As seen in Sec. III-B, interference is expected to dominate the thermal noise for very large densities. The trend for downlink SINR coverage for such densities is shown in Fig. 8 for lightly ($C = 0.5$) and densely blocked ($C = 0.12$) scenarios. All BSs are assumed to be transmitting in Fig. 8a, whereas BSs only with a user in the corresponding association cell are assumed to be transmitting in Fig. 8b. The coverage for the latter case is obtained by thinning the interference field by probability $1 - K(\lambda_u, \lambda, 0)$ (details in Appendix B). As can be seen, ignoring the finite user population, the SINR coverage saturates, where that saturation is achieved quickly for lightly blocked scenarios—a trend corroborated by the observations of [23]. However, accounting for the finite user population leads to an *opposite* trend, as the increasing density monotonically improves the path loss to the tagged BS but the interference

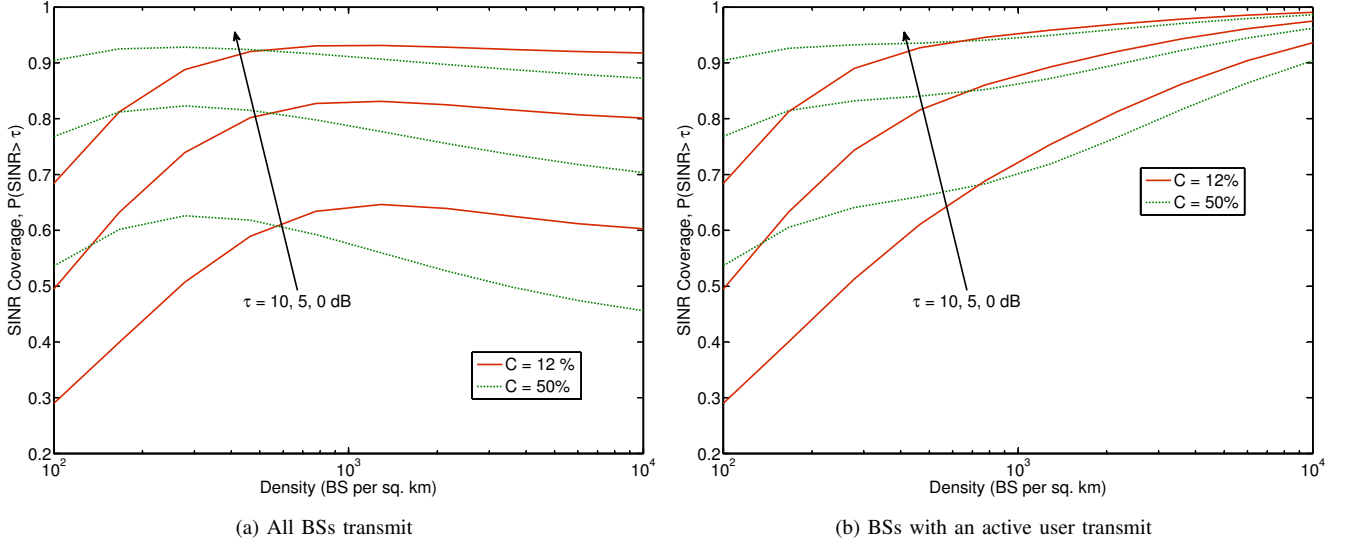


Fig. 8: SINR coverage variation with large densities for different blockage densities.

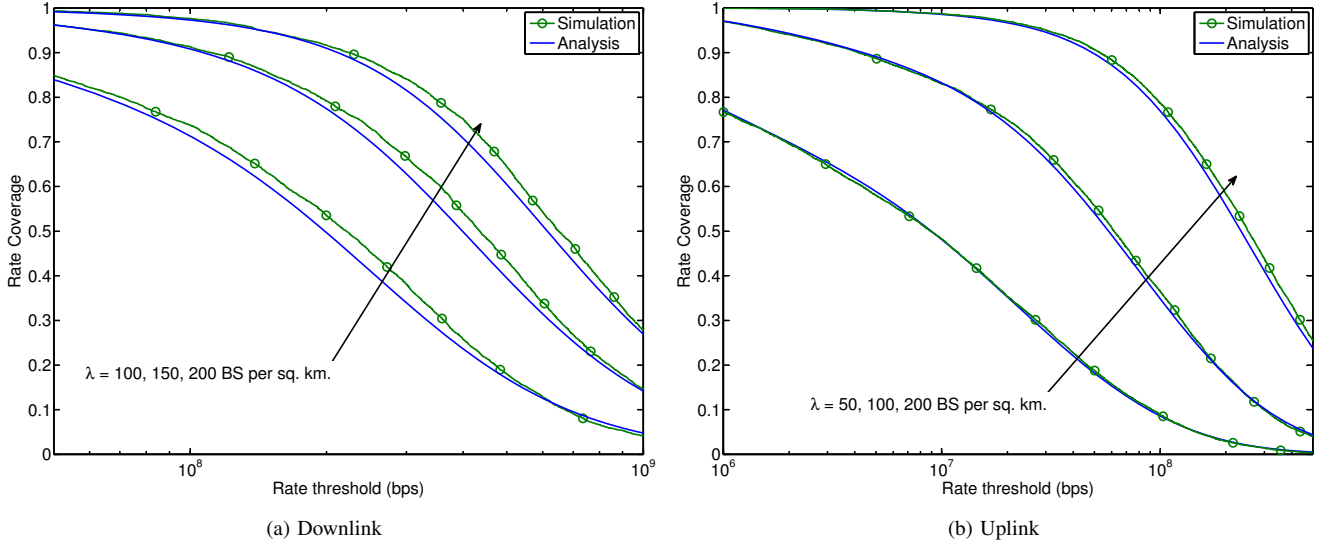


Fig. 9: Downlink and uplink rate coverage for different BS densities and fixed $\omega = 0.5$.

is (implicitly) capped by the finite user density of 1000 per sq. km.

B. Rate coverage

The variation of downlink and uplink rate distribution with the density of infrastructure for a fixed A-BS fraction $\omega = 0.5$ is shown in Fig 9. Reducing the cell size by increasing density boosts the coverage and decreases the load per base station. This dual benefit improves the overall rate drastically with density as shown in the plot. Further, the good match of analytical curves to that of simulation also validates the analysis for uplink and downlink rate coverage.

The variation in rate distribution with bandwidth is shown in Fig. 10 for a fixed BS density $\lambda = 100$ BS per sq. km and $\omega = 1$. Two observations can be made here: 1) median and peak rate increase considerably with the availability of larger

bandwidth, whereas 2) cell edge rates exhibit a non-increasing trend. The latter trend is due to the low SNR of the cell edge users, where the gain from bandwidth is counterbalanced by the loss in SNR. Further, if the constraint of Rate = 0 for $\text{SNR} < \tau_0$ is imposed, cell edge rates would actually decrease as shown in Fig. 10b due to the increase in $\mathbb{P}(\text{SNR} < \tau_0)$, highlighting the impossibility of increasing rates for power-limited users in mmW networks by just increasing the system bandwidth. In fact, it may be counterproductive.

C. Impact of co-existence

The rate distribution of a mmW only network and that of a mmW- μ W hybrid network is shown in Fig. 11 for different mmW BS densities and fixed μ W network density of $\mu = 5$ BS per sq. km. Offloading users from mmW to μ W, when the link SNR drops below $\tau_{\min} = -10$ dB improves the

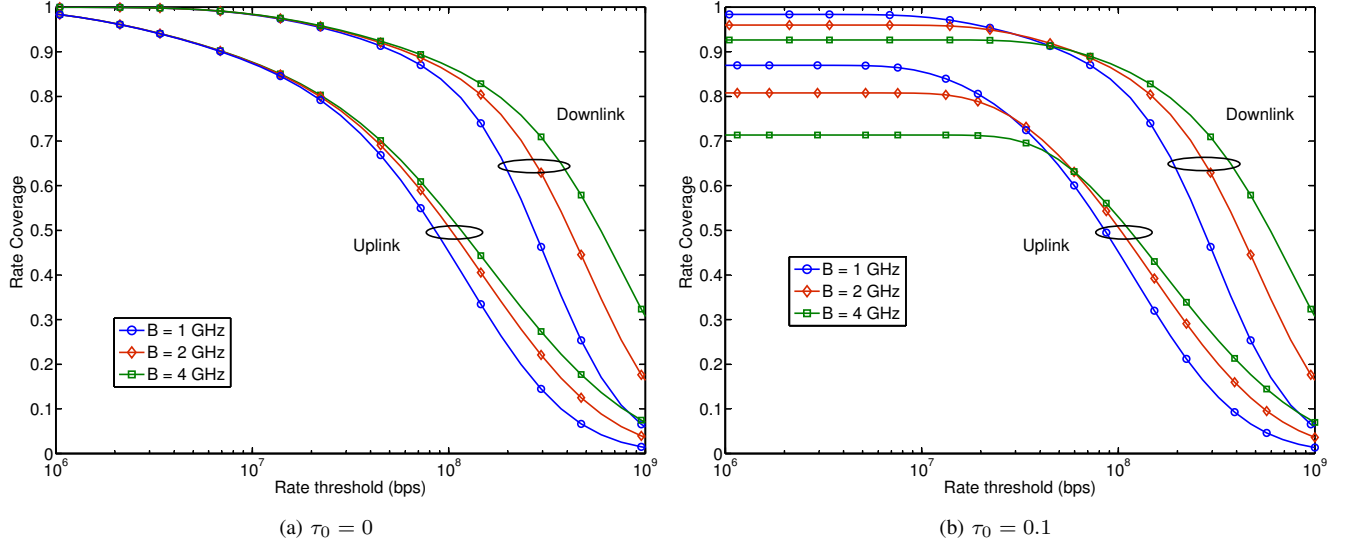


Fig. 10: Effect of bandwidth and min SNR constraint (Rate = 0 for $\text{SNR} < \tau_0$) on rate distribution for BS density 100 per sq. km.

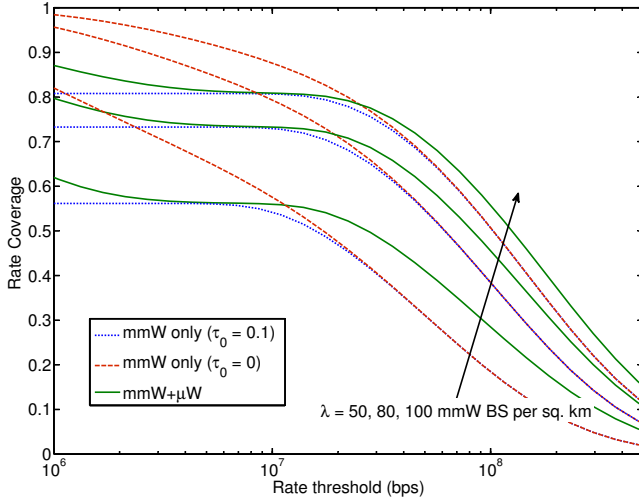


Fig. 11: Downlink rate distribution for mmW only and hybrid network for different mmW BS density and fixed μW density of 5 BS per sq. km.

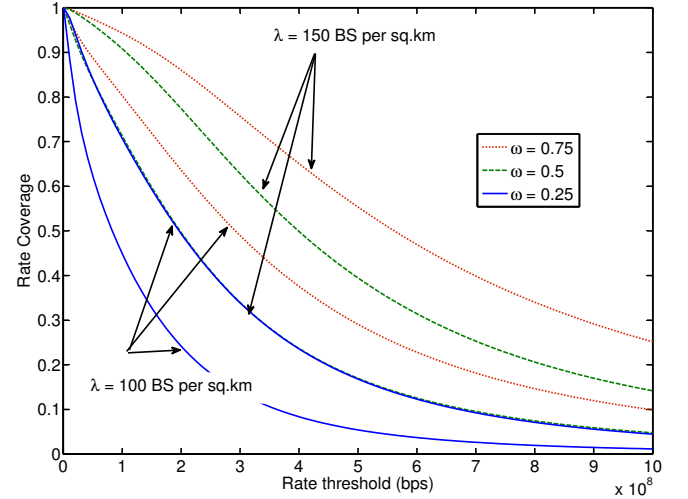


Fig. 12: Rate distribution with variation in ω

rate of edge users significantly, when the min SNR constraint ($\tau_0 = -10$ dB) is imposed. Such gain from co-existence, however, reduces with increasing mmW BS density, as the fraction of “poor” SNR users reduces. Without any such minimum SNR consideration, i.e., $\tau_0 = 0$, mmW is preferred due to the 100x larger bandwidth. So the key takeaway here is that users should be offloaded to a co-existing μW macrocellular network only when reliable communication over the mmW link is unfeasible.

D. Impact of self-backhauling

The variation of downlink rate distribution with the fraction of A-BSs ω in the network with BS density of 100 and 150 per sq. km is shown in Fig. 12. As can be seen, providing wired backhaul to increasing fraction of BSs improves the overall

rate distribution. However “diminishing return” is seen with increasing ω as the bottleneck shifts from the backhaul to the air interface rate. Further, it can be observed from the plot that different combinations of A-BS fraction and BS density, e.g. ($\omega = 0.25, \lambda = 150$) and ($\omega = 0.5, \lambda = 100$) lead to similar rate distribution. This is investigated further using Lemma 2 in Fig. 13, which characterizes the different contours of (ω, λ) required to guarantee various median rates ρ_{50} ($\mathcal{R}(\rho_{50}) = 0.5$) in the network. For example, a median rate of 400 Mbps in the network can be provided by either $\omega = 0.9, \lambda = 110$ or $\omega = 0.3, \lambda = 200$. Thus, the key insight from these results is that it is feasible to provide the same QoS (median rate here) in the network by either providing wired backhaul to a small fraction of BSs in a dense network, or by increasing the corresponding fraction in a sparser network. In the above plots, the actual number of A-BSs in a given area increased with increasing density for a fixed ω , but if the density of

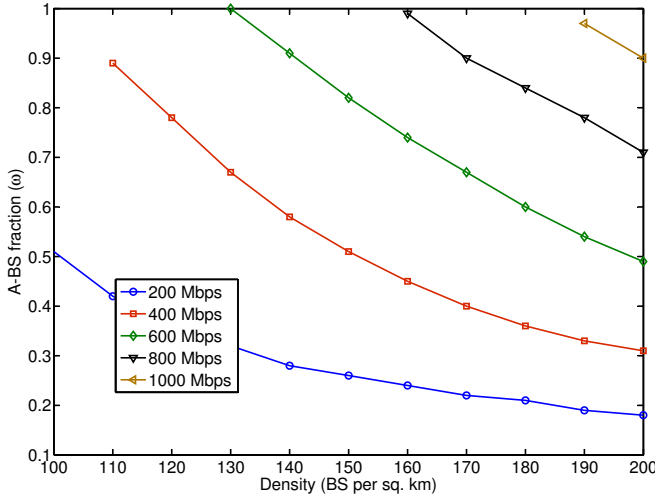


Fig. 13: The required ω for achieving different median rates with varying density

A-BSs is fixed (γ , say) while increasing the density of BSs, i.e., $\omega = \frac{\gamma}{\lambda}$ for some constant γ , would a similar trend as the earlier plot be seen? This can be answered by a closer look at Lemma 2. With increasing λ , the rate coverage of the access link increases shifting the bottleneck to backhaul link, which in turn is limited by the A-BS density. This notion is formalized in the following proposition.

Proposition 3. We define the saturation density $\lambda_{\text{sat}}^{\delta}(\gamma)$ as the density beyond which only marginal ($\delta\%$ at most) gain in rate coverage can be obtained with A-BS density fixed at γ , and characterized as

$$\lambda_{\text{sat}}^{\delta}(\gamma) : \inf_{\lambda} \|S_d \left(v \left\{ \hat{\rho} 1.28 \frac{\lambda_u}{\lambda} \right\} \right) - 1\| \leq \delta / S_b \left(v \left\{ \hat{\rho} 1.28^2 \frac{\lambda_u}{\gamma} \right\} \right). \quad (7)$$

Proof: As the contribution from the access rate coverage can be at most 1, the saturation density is characterized from Corollary 1 as

$$\lambda_{\text{sat}}^{\delta}(\gamma) : \inf_{\lambda} \|S_d \left(v \left\{ \hat{\rho} \left(1 + 1.28 \frac{\lambda_u}{\lambda} \right) \frac{2\gamma + 1.28(\lambda - \gamma)}{\gamma + 1.28(\lambda - \gamma)} \right\} \right) - 1\| \leq \delta S_b \left(v \left\{ \hat{\rho} \left(1 + 1.28 \frac{\lambda_u}{\lambda} \right) \left(2 + 1.28 \frac{\lambda - \gamma}{\gamma} \right) \right\} \right)^{-1}.$$

Noticing $\lambda \gg \gamma$ and $\lambda_u \gg \lambda$ leads to the result. ■

From (7), it is clear that $\lambda_{\text{sat}}^{\delta}(\gamma)$ increases with γ , as RHS decreases. For various values of A-BS density, Fig. 14 shows the variation in rate coverage with BS density for a rate threshold of 100 Mbps. As postulated above, the rate coverage saturates with increasing density for each A-BS density. Also shown is the saturation density obtained from (7) for a margin δ of 2%. Further, saturation density is seen to be increasing with the A-BS density, as more BSs are required for access rate to dominate the increasing backhaul rate.

V. CONCLUSION AND FUTURE CHALLENGES

A baseline model and analytical framework is presented for characterizing the rate distribution in mmW cellular networks. To the best of authors' knowledge, the presented work is the first to integrate self-backhauling among BSs and co-existence

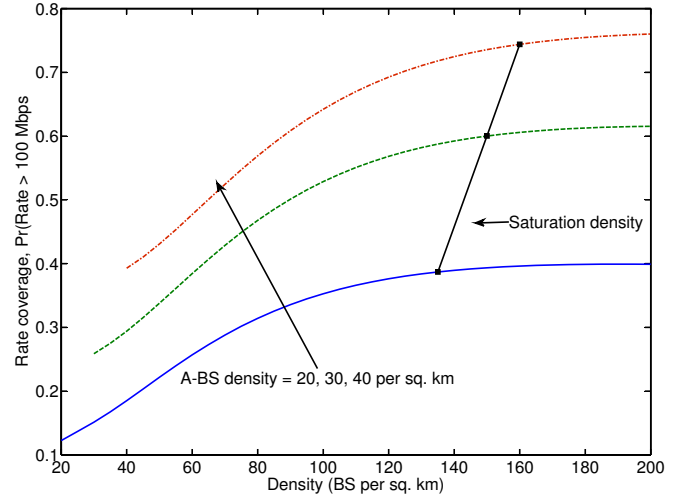


Fig. 14: Rate distribution with variation in BS density but fixed A-BS density.

with a conventional macrocellular network into the analysis of mmW networks. We show that bandwidth plays minimal impact on the rate of power and noise-limited cell edge users, whereas increasing the BS density improves the corresponding rates drastically. This paper also further establishes the noise-limited nature of large bandwidth mmW networks. With self-backhauling, the rate saturates with increasing BS density for fixed A-BS density, where the corresponding saturation density is directly proportional to the A-BS density. The explicit characterization of the rate distribution as a function of key system parameters, which we provide, should help advance further the understanding of such networks and benchmark their performance.

The presented work can be extended in a number of directions. Offloading of indoor users, which may not even receive the signal from outdoor mmW BSs, to more stable networks like 4G or WiFi could be further investigated. Allowing multihop backhaul in sparser deployment of A-BSs could also be investigated in future work. The developed analytical framework also provides tools to analyze other network architectures like device-to-device (D2D) and ad hoc mmW networks.

ACKNOWLEDGMENT

The authors appreciate feedback from X. Zhang.

APPENDIX A

Derivation of path loss distribution: We drop the subscript 'a' for access in this proof. The propagation process $\mathcal{N} := L(X) = S(X)^{-1} \|X\|^{\alpha(X)}$ on \mathbb{R} for $X \in \Phi$, where $S \triangleq 10^{-(\alpha+\beta)/10}$, has the intensity measure

$$\Lambda((0, t]) = \int_{\mathbb{R}^2} \mathbb{P}(L(X) < t) dX = 2\pi\lambda \int_{\mathbb{R}^+} \mathbb{P}\left(\frac{r^{\alpha(r)}}{S(r)} < t\right) r dr.$$

Denote a link to be of type j , where $j = l$ (LOS) and $j = n$ (NLOS) with probability $C_{j,D}$ for link length less than D and

$C_{j,\bar{D}}$ otherwise. Note by construction $C_{l,D} + C_{n,D} = 1$ and $C_{l,\bar{D}} + C_{n,\bar{D}} = 1$. The intensity measure is then

$$\begin{aligned}\Lambda((0, t]) &= 2\pi\lambda \sum_{j \in \{l, n\}} C_{j,D} \int_{\mathbb{R}^+} \mathbb{P}\left(\frac{r^{\alpha_j}}{S_j} < t\right) \mathbb{1}(r < D) r dr \\ &+ C_{j,\bar{D}} \int_{\mathbb{R}^+} \mathbb{P}\left(\frac{r^{\alpha_j}}{S_j} < t\right) \mathbb{1}(r > D) r dr \\ &= 2\pi\lambda \mathbb{E}\left[\sum_{j \in \{l, n\}} (C_{j,D} - C_{j,\bar{D}}) \frac{D^2}{2} \mathbb{1}(S_j > D^{\alpha_j}/t)\right. \\ &+ C_{j,D} \frac{(tS_j)^{2/\alpha_j}}{2} \mathbb{1}(S_j < D^{\alpha_j}/t) + C_{j,\bar{D}} \frac{(tS_j)^{2/\alpha_j}}{2} \mathbb{1}(S_j > D^{\alpha_j}/t)\Big] \\ &= \lambda\pi \sum_{j \in \{l, n\}} (C_{j,D} - C_{j,\bar{D}}) D^2 \bar{F}_{S_j}(D^{\alpha_j}/t) \\ &+ t^{2/\alpha_j} \left(C_{j,D} \bar{\zeta}_{S_j, 2/\alpha_j}(D^{\alpha_j}/t) + C_{j,\bar{D}} \zeta_{S_j, 2/\alpha_j}(D^{\alpha_j}/t)\right),\end{aligned}$$

where \bar{F}_S denotes the CCDF of S , and $\bar{\zeta}_{S,n}(x), \zeta_{S,n}(x)$ denote the truncated n^{th} moment of S given by $\bar{\zeta}_{S,n}(x) \triangleq \int_0^x s^n f_S(s) ds$ and $\zeta_{S,n}(x) \triangleq \int_x^\infty s^n f_S(s) ds$. Since S is a Lognormal random variable $\sim \ln \mathcal{N}(m, \sigma^2)$, where $m = -0.1\beta \ln 10$ and $\sigma = 0.1\xi \ln 10$. The intensity measure in Lemma 1 is then obtained by using

$$\begin{aligned}\bar{F}_S(x) &= Q\left(\frac{\ln x - m}{\sigma}\right), \\ \bar{\zeta}_{S,n}(x) &= \exp(\sigma^2 n^2/2 + mn) Q\left(\frac{\sigma^2 n - \ln x + m}{\sigma}\right) \\ \zeta_{S,n}(x) &= \exp(\sigma^2 n^2/2 + mn) Q\left(-\frac{\sigma^2 n - \ln x + m}{\sigma}\right).\end{aligned}$$

Now, since \mathcal{N} is a PPP, the distribution of path loss to the tagged BS is then $\mathbb{P}(\inf_{X \in \Phi} L(X) > t) = \Lambda((0, t])$. ■

APPENDIX B

SINR distribution: Having derived the intensity measure of \mathcal{N} in Lemma 1, the distribution of SINR can be characterized on the same lines as [36]. The key steps are highlighted below for completeness.

$$\begin{aligned}\mathbb{P}(\text{SINR} > \tau) &= \mathbb{P}\left(\frac{P_b G_{\max} L(X^*)^{-1}}{\sum_{X \in \Phi \setminus \{X^*\}} P_b \psi_X L(X)^{-1} + \sigma_N^2} > \tau\right) \\ &= \mathbb{P}\left(J + \frac{\sigma_N^2 L(X^*)}{P_b G_{\max}} < \frac{1}{\tau}\right) \\ &= \int_{l>0} \mathbb{P}\left(J + \frac{\sigma_N^2 l}{P_b G_{\max}} < \frac{1}{\tau} \mid L(X^*) = l\right) f_{L(X^*)}(l) dl\end{aligned}$$

where $J = \frac{L(X^*)}{G_{\max}} \sum_{X \in \Phi \setminus \{X^*\}} \psi_X L(X)^{-1}$ and the distribution of $L(X^*)$ is derived as

$$f_{L(X^*)}(l) = -\frac{d}{dl} \mathbb{P}(L(X^*) > l) = \lambda \exp(-\lambda M(l)) M'(l). \quad (8)$$

The conditional CDF required for the above computation is derived from the conditional Laplace transform given below using the Euler's characterization [37]

$$\begin{aligned}\mathcal{L}_{J,l}(z) &= \mathbb{E}[\exp(-zJ) \mid L(X^*) = l] \\ &= \exp\left(-\mathbb{E}_\psi \left[\int_{u>l} (1 - \exp(-zl\psi/u)) \Lambda(du)\right]\right),\end{aligned}$$

where $\Lambda(du)$ is given by (4).

The inverse Laplace transform calculation required in the above derivation could get computationally intensive in certain cases and may render the analysis intractable. However, introducing Rayleigh small scale fading $H \sim \exp(1)$, on each link improves the tractability of the analysis as shown below. Coverage with fading is

$$\begin{aligned}&\mathbb{P}\left(\frac{P_b G_{\max} H_{X^*} L(X^*)^{-1}}{\sum_{X \in \Phi \setminus \{X^*\}} P_b \psi_X H_X L(X)^{-1} + \sigma_N^2} > \tau\right) \\ &= \mathbb{E}\left[\exp\left(-\frac{\tau \sigma_N^2}{P_b G_{\max}} L(X^*) - \tau L_{X^*} \sum_{X \in \Phi \setminus \{X^*\}} \frac{\psi_X}{G_{\max}} H_X L(X)^{-1}\right)\right] \\ &\stackrel{(a)}{=} \int_{l>0} \exp\left(-\frac{\tau \sigma_N^2}{P_b G_{\max}} l - \lambda \mathbb{E}_z \left[\int_{u>l} \frac{M'(u) du}{u(zl)^{-1} + 1}\right]\right) f_{L_{X^*}}(l) dl \\ &\stackrel{(b)}{=} \lambda \int_{l>0} \exp\left(-\frac{\tau \sigma_N^2}{P_b G_{\max}} l - \lambda M(l) \mathbb{E}_\psi \left[\frac{1}{1+z}\right]\right) \\ &\quad \times \exp\left(-\lambda \mathbb{E}_\psi \left[\int_0^{\frac{z}{z+1}} M\left\{zl\left(\frac{1}{u} - 1\right)\right\} du\right]\right) M'(l) dl\end{aligned}$$

where $z = \frac{\tau \psi}{G_{\max}}$, (a) follows using the Laplace functional of point process \mathcal{N} , (b) follows using integration by parts along with (8).

The above derivation assumed all BSs to be transmitting, but since user population is finite, certain BSs may not have a user to serve with probability $1 - K(\lambda_u, \lambda, 0)$. This is incorporated in the analysis by modifying $\lambda \rightarrow \lambda(1 - K(\lambda_u, \lambda, 0))$ in (a) above. ■

REFERENCES

- [1] FCC, "National broadband plan recommendations." Available at: <http://www.broadband.gov/plan/5-spectrum/r5>.
- [2] Cisco, "Cisco visual networking index: Global mobile data traffic forecast update, 2012-2017." Whitepaper, available at: <http://goo.gl/xxLT>.
- [3] F. Boccardi, R. W. Heath, A. Lozano, T. L. Marzetta, and P. Popovski, "Five disruptive technology directions for 5G," *IEEE Commun. Mag.*, vol. 52, pp. 74–80, Feb. 2014.
- [4] T. Rappaport *et al.*, "Millimeter wave mobile communications for 5G cellular: It will work!," *IEEE Access*, vol. 1, pp. 335–349, May 2013.
- [5] J. G. Andrews *et al.*, "What will 5G be?," *IEEE J. Sel. Areas Commun.*, vol. PP, June 2014.
- [6] T. Baykas *et al.*, "IEEE 802.15.3c: The first IEEE wireless standard for data rates over 1 Gb/s," *IEEE Commun. Mag.*, vol. 49, pp. 114–121, July 2011.
- [7] R. C. Daniels, J. N. Murdock, T. S. Rappaport, and R. W. Heath, "60 GHz wireless: Up close and personal," *IEEE Microw. Mag.*, vol. 11, pp. 44–50, Dec. 2010.
- [8] Z. Pi and F. Khan, "An introduction to millimeter-wave mobile broadband systems," *IEEE Commun. Mag.*, vol. 49, pp. 101–107, June 2011.
- [9] W. Roh *et al.*, "Millimeter-wave beamforming as an enabling technology for 5G cellular communications: Theoretical feasibility and prototype results," *IEEE Commun. Mag.*, vol. 52, pp. 106–113, Feb. 2014.
- [10] T. Rappaport *et al.*, "Broadband millimeter-wave propagation measurements and models using adaptive-beam antennas for outdoor urban cellular communications," *IEEE Trans. Antennas Propag.*, vol. 61, pp. 1850–1859, Apr. 2013.
- [11] S. Rangan, T. Rappaport, and E. Erkip, "Millimeter-wave cellular wireless networks: Potentials and challenges," *Proceedings of the IEEE*, vol. 102, pp. 366–385, Mar. 2014.
- [12] M. R. Akdeniz *et al.*, "Millimeter wave channel modeling and cellular capacity evaluation," *IEEE J. Sel. Areas Commun.*, vol. PP, June 2014.
- [13] S. Larew, T. Thomas, and A. Ghosh, "Air interface design and ray tracing study for 5G millimeter wave communications," *IEEE Globecom B4G Workshop*, pp. 117–122, Dec. 2013.
- [14] A. Ghosh *et al.*, "Millimeter wave enhanced local area systems: A high data rate approach for future wireless networks," *IEEE J. Sel. Areas Commun.*, vol. PP, June 2014.

- [15] M. Abouelseoud and G. Charlton, "System level performance of millimeter-wave access link for outdoor coverage," in *IEEE WCNC*, pp. 4146–4151, Apr. 2013.
- [16] S. Singh, R. Mudumbai, and U. Madhow, "Interference analysis for highly directional 60 GHz mesh networks: The case for rethinking medium access control," *IEEE/ACM Trans. Netw.*, vol. 19, pp. 1513–1527, Oct. 2011.
- [17] Interdigital, "Small cell millimeter wave mesh backhaul," Feb. 2013. Whitepaper, available at: <http://goo.gl/DI2Z6V>.
- [18] R. Taori and A. Sridharan, "In-band, point to multi-point, mm-Wave backhaul for 5G networks," in *IEEE Intl. Workshop on 5G Tech., ICC*, June 2014.
- [19] J. S. Kim, J. S. Shin, S.-M. Oh, A.-S. Park, and M. Y. Chung, "System coverage and capacity analysis on millimeter-wave band for 5G mobile communication systems with massive antenna structure," *Intl. Journal of Antennas and Propagation*, vol. 2014, July 2014.
- [20] M. Coldrey, J.-E. Berg, L. Manholm, C. Larsson, and J. Hansryd, "Non-line-of-sight small cell backhauling using microwave technology," *IEEE Commun. Mag.*, vol. 51, pp. 78–84, Sept. 2013.
- [21] S. W. Peters, A. Y. Panah, K. T. Truong, and R. W. Heath, "Relay architectures for 3GPP LTE-advanced," *EURASIP Journal on Wireless Communications and Networking*, 2009.
- [22] S. Akoum, O. El Ayach, and R. Heath, "Coverage and capacity in mmWave cellular systems," in *Asilomar Conference on Signals, Systems and Computers (ASILOMAR)*, pp. 688–692, Nov. 2012.
- [23] T. Bai and R. W. Heath, "Coverage and rate analysis for millimeter wave cellular networks," *IEEE Trans. Wireless Commun.*, 2014. Submitted, available at <http://arxiv.org/abs/1402.6430>.
- [24] T. Bai and R. W. Heath, "Coverage analysis for millimeter wave cellular networks with blockage effects," in *IEEE Global Conf. on Signal and Info. Processing (GlobalSIP)*, pp. 727–730, Dec. 2013.
- [25] T. Bai, R. Vaze, and R. W. Heath, "Analysis of blockage effects on urban cellular networks," *IEEE Trans. Wireless Commun.*, 2014. To appear. Available at: <http://arxiv.org/abs/1309.4141>.
- [26] S. Singh, H. S. Dhillon, and J. G. Andrews, "Offloading in heterogeneous networks: Modeling, analysis, and design insights," *IEEE Trans. Wireless Commun.*, vol. 12, pp. 2484–2497, May 2013.
- [27] J. G. Andrews, S. Singh, Q. Ye, X. Lin, and H. S. Dhillon, "An overview of load balancing in HetNets: Old myths and open problems," *IEEE Wireless Commun. Mag.*, vol. 21, pp. 18–25, Apr. 2014.
- [28] The City of New York, "New York building perimeter data." Online, available at: <http://tinyurl.com/khlo69r>.
- [29] The City of Chicago, "Chicago building perimeter data." Online, available at: <http://tinyurl.com/mccksq4>.
- [30] A. Guo and M. Haenggi, "Asymptotic deployment gain: A simple approach to characterize the SINR distribution in general cellular networks," *IEEE Trans. Commun.*, 2014. Submitted, available at: <http://arxiv.org/abs/1404.6556>.
- [31] S. Yi, Y. Pei, and S. Kalyanaraman, "On the capacity improvement of ad hoc wireless networks using directional antennas," in *Intl. Symp. on Mobile Ad Hoc Networking and Computing, MobiHoc*, pp. 108–116, 2003.
- [32] H. Wang and M. Reed, "Tractable model for heterogeneous cellular networks with directional antennas," in *Australian Communications Theory Workshop (AusCTW)*, pp. 61–65, Jan. 2012.
- [33] J. Wildman, P. H. J. Nardelli, M. Latva-aho, and S. Weber, "On the joint impact of beamwidth and orientation error on throughput in wireless directional Poisson networks," *IEEE Trans. Wireless Commun.*, 2014. To appear, available at: <http://arxiv.org/abs/1312.6057>.
- [34] F. Baccelli and B. Blaszczyzyn, *Stochastic Geometry and Wireless Networks, Volume I – Theory*. NOW: Foundations and Trends in Networking, 2009.
- [35] Q. C. Li, H. Niu, G. Wu, and R. Q. Hu, "Anchor-booster based heterogeneous networks with mmWave capable booster cells," *IEEE Globecom B4G Workshop*, Dec 2013.
- [36] B. Blaszczyzyn, M. K. Karray, and H.-P. Keeler, "Using Poisson processes to model lattice cellular networks," in *Proc. IEEE Intl. Conf. on Comp. Comm. (INFOCOM)*, pp. 773–781, Apr. 2013.
- [37] J. Abate and W. Whitt, "Numerical inversion of Laplace transforms of probability distributions," *ORSA Journal on Computing*, vol. 7, no. 1, pp. 36–43, 1995.
- [38] S. Singh, "Matlab code for numerical computation of total power to noise ratio in mmW networks." [Online]. Available : <http://goo.gl/MF9qfd>.
- [39] S. Singh, F. Baccelli, and J. G. Andrews, "On association cells in random heterogeneous networks," *IEEE Wireless Commun. Lett.*, vol. 3, pp. 70–73, Feb. 2014.
- [40] J.-S. Ferenc and Z. Nédá, "On the size distribution of Poisson Voronoi cells," *Physica A: Statistical Mechanics and its Applications*, vol. 385, pp. 518 – 526, Nov. 2007.
- [41] S. M. Yu and S.-L. Kim, "Downlink capacity and base station density in cellular networks," in *Intl. Symp. on Modeling Optimization in Mobile Ad Hoc Wireless Networks (WiOpt)*, pp. 119–124, May 2013.
- [42] J. G. Andrews, F. Baccelli, and R. K. Ganti, "A tractable approach to coverage and rate in cellular networks," *IEEE Trans. Commun.*, vol. 59, pp. 3122–3134, Nov. 2011.